Author for correspondence:
Haijun Hu
e-mail: huhaijun@mail.xjtu.edu.cn

ROYAL SOCIETY OF CHEMISTRY

THE ROYAL SOCIETY PUBLISHING

Corrosion resistance of graphene/waterborne epoxy composite coatings in CO$_2$-satarated NaCl solution

Hao Xu[1], Haijun Hu[1], Hongmei Wang[2], Yongjun Li[2] and Yun Li[1]

[1]Department of Process Equipment and Control Engineering, Xi'an Jiaotong University, Xi'an 710049, People's Republic of China
[2]Gas Production Technology Research Institute, NO.1 Gas Production Plant of Changqing Oilfield Company, Jingbian 718500, People's Republic of China

HX, 0000-0002-9277-1886

This study investigated the corrosion resistance of graphene/waterborne epoxy composite coatings in CO$_2$-satarated NaCl solution. The coatings were prepared by dispersing graphene in waterborne epoxy with the addition of carboxymethylcellulose sodium. The structure and composition of the coatings were characterized by scanning electron microscopy, transmission electron microscopy, Fourier-transform infrared and Raman spectroscopies. The corrosion resistance of the composite coatings was investigated by potentiodynamic polarization measurements and electrochemical impedance spectroscopy. Composite coatings with more uniform surfaces and far fewer defects than blank waterborne epoxy coatings were obtained on 1020 steel. The 0.5 wt% graphene/waterborne epoxy composite coating exhibited a much lower corrosion rate and provided better water resistance properties and long-term protection than those of the blank epoxy coating in CO$_2$-satarated NaCl solution.

1. Introduction

The CO$_2$ corrosion of pipelines is attracting more and more attention in the oil and gas industry because of the CO$_2$-enhanced oil recovery [1]. In this process, by injecting CO$_2$ into oil and gas fields, the residual oil and gas can be pushed out to improve oil recovery. CO$_2$ corrosion is the main form of internal corrosion failure in oil and natural gas pipelines [2]. During the CO$_2$ flooding test in the Little Creek Oilfield, USA, the wall of the oil extraction pipe was corroded and perforated within five months with a corrosion rate of 12.7 mm yr^{-1} [3]. Pipeline corrosion resulted in billions of dollars in losses to the oil and

Table 1. Chemical composition of the 1020 steel used for the experiments (wt%).

C	Si	Mn	P	S	Ni	Cr	Cu	Fe
0.17–0.23	0.17–0.37	0.35–0.65	≤0.035	≤0.035	≤0.30	≤0.25	≤0.25	balance

gas industry. Numerous reports have shown that the rupture of oil and gas pipelines caused by corrosion has resulted in oil spillages causing environmental pollution. Further ecological damage and economic losses are then caused by dealing with such environmental pollution [4,5].

These losses associated with CO_2 have promoted studies on corrosion prevention methods in the oil and gas industry. Coatings [6], inhibitors [7,8] and adding alloying elements [9,10] are the most common strategies to minimize corrosion of the substrate metal. In particular, organic coatings have been considered as an effective way to retard corrosion owing to their excellent properties and stability.

Traditional organic coatings are mainly solvent based. The release of volatile organic compounds during the coating and service processes can be harmful to the environment and the health of construction workers. Unfortunately, the protective effects of waterborne coatings, such as their film-forming properties, water resistance properties and shielding properties, are significantly lower than those of solvent-based coatings. We therefore considered adding graphene to improve the corrosion resistance of waterborne epoxy coatings for application in oil and gas industry environments.

Graphene is a flat film carbon material that is composed of monolayer sp^2-hybridized carbon atoms. Graphene has high thermal and chemical stability and can isolate the substrate from the corrosive medium to provide effective corrosion inhibition [11]. Chen et al. [12] first studied the antioxidant capacity of graphene grown on the surface of pure Cu and a Cu/Ni alloy through chemical vapour deposition (CVD). It has been reported that graphene obtained through CVD can tremendously improve the resistance of the base metal to corrosion in a short time [13–16], however, CVD cannot yield defect-free graphene films. Over the long term, O_2 and H_2O molecules will penetrate through the defects and corrode the metal substrate [17].

Many reports have indicated that graphene composite coatings can provide considerable corrosion inhibition. The addition of graphene and functionalized graphene in organic coatings can further improve the corrosion performance in marine environments [18–20]. Ye et al. [21] intercalated the silanized trianiline precursor into graphene sheets to prepare the aniline trimer (AT)-functionalized graphene (SAT-G). The silanized AT could disperse graphene sheets in the epoxy resin more effectively. The composite epoxy matrix could provide much better corrosion resistance over the long term by adding the appropriate amount of SAT-G (0.5 wt%). Yang et al. [22] synthesized the 3,4,9,10-perylene tetracarboxylic acid-graphene (PTCA-G) composite and investigated the anti-corrosion properties of composite coatings containing PTCA-G. The composite coating showed excellent corrosion resistance when containing the PTCA-G composite with a 10 : 4 volume ratio of PTCA and G.

Although graphene-reinforced epoxy coatings have shown improved corrosion resistance in many applications, there is still a lack of relevant research in oil and gas production environments where aggressive CO_2 and sometimes high concentrations of Cl^- are both present. In this study, we investigated the corrosion resistance of graphene/waterborne epoxy composite coatings in CO_2-saturated NaCl solution and discussed the corrosion mechanism of the composite coatings.

2. Experimental

2.1. Material and methods

Around 1020 steel specimens were cut into 10 mm × 10 mm × 2 mm and then sealed in epoxy resin with an exposure area of 1 cm^2 (10 mm × 10 mm) for electrochemical measurements. The chemical composition of 1020 steel used in this study is shown in table 1. Prior to coating, the test surfaces of the specimens were abraded using sandpaper with grit grades of 280, 400, 600, 800, 1200 and 1500. The surfaces were then polished with a flannel polishing cloth (≤1 μm), degreased with ethanol and washed with deionized water. The prepared specimens were stored in a desiccator before testing.

F0704 two-component waterborne epoxy was purchased from Dongguan Rongzhong Chemical Co., Ltd. Graphene powder (purity: 99.7%, 4–7 nm/6 × 6 μm) was purchased from Beijing Forsman Technology Co., Ltd. Diamino-functionalized polyethylene glycol (NH2-PEG-NH2, purity ≥ 95%) was purchased from Dongguan Aoda Co., Ltd. Carboxymethylcellulose sodium (CMC)

(viscosity:1500–3100 mpa.s, USP grade), fumed silica (purity: 99.8%) and other reagents were supplied from Shanghai Macklin Biochemical Co., Ltd.

2.2. Electrolyte composition

According to the composition data collected from a gas production plant site, the Cl^- concentration in formation water can be as high as $60\,000$–$100\,000\,mg\,l^{-1}$. Therefore, electrochemical experiments were conducted in high chloride environment aqueous solutions with 10 wt% NaCl at 25°C and atmospheric pressure. The electrolyte solution was purged with CO_2 for 8 h to deoxygenate and saturate with CO_2 before the specimen was inserted into the solution. CO_2 was continuously introduced into the electrolyte solution during the electrochemical experiment.

2.3. Preparation of graphene/waterborne epoxy composite coating

The composite coatings were prepared by the dispersion of different mass fractions of graphene in waterborne epoxy matrix. CMC was used as the dispersant and fumed silica was used as the anti-sediment agent. Different weight ratios (0%, 0.25% and 0.50%) of graphene and a small amount of diamino-functionalized polyethylene glycol were added into the waterborne epoxy and the composite was then dispersed by ultrasonication for 0.5 h. Epoxy curing agent was added with a 2 : 1 weight ratio of epoxy matrix and curing agent. Then, the composite was dispersed by ultrasonication for another 0.5 h and uniformly coated on the test surface of 1020 steel using a wire bar coater (20 µm). The sample was then cured at 25°C for 24 h.

2.4. Characterization of coatings

An infrared spectrometer (Nicolet iS50) was used to record the Fourier-transform infrared (FTIR) spectra. Raman spectra were collected on a laser Raman spectrometer (LabRAM HR Evolution). Scanning electron microscopy (SEM) images were recorded on using an MAIA3 LMH microscope. In order to characterize the microscopic morphology of the graphene and composite coatings, an FEI Tecnai G2 F20 microscope was employed to collect the transmission electron microscopy (TEM) images.

2.5. Electrochemical measurements

The anti-corrosion properties of different coatings in CO_2-satarated NaCl solution were studied by measurements of polarization curve and electrochemical impedance spectroscopy (EIS). A glass cell equipped with a three-electrode system was employed in this study. The working electrode was a bare or coated steel 1020 specimen. A platinum electrode was employed as the counter electrode and a saturated calomel electrode was used as the reference electrode. The polarization curves were collected from $-0.45\,V$ to $0.45\,V$ versus open circuit potential at the scan rate of $0.5\,mV\,s^{-1}$ and fitted by CVIEW 2.6. The EIS data were recorded from 100 kHz to 0.01 Hz with a 40 mV amplitude signal and fitted by ZSIMPWIN 3.30d. Electrochemical workstation (CS350) was used to carry out all electrochemical tests.

3. Results and discussion

3.1. Characterization of composite coatings

Raman spectra were recorded to identify if interactions between the CMC and graphene sheets occurred during coating preparation. In figure 1a, the pristine graphene exhibited two characteristic peaks corresponding to the G band at $1583\,cm^{-1}$ and the D band at $1345\,cm^{-1}$, respectively [23,24]. The G band corresponds to the structure of sp^2-bonding carbon atoms, while the D-band is owing to the breaking mode near the K zone boundary [25].

Graphene dispersed by CMC is referred to as CMC–graphene in the rest of this paper. The Raman spectrum of CMC–graphene is shown in figure 1b. The G band for graphene ($1583\,cm^{-1}$) was blue-shifted to $1586\,cm^{-1}$ for CMC–graphene, indicating strong interaction between the CMC and graphene sheets. The integral areas value of the D band to G band (I_D/I_G) was used to evaluate the quality of graphene sheets. The I_D/I_G ratio of pristine graphene was 1.12 which increased to 1.25 for
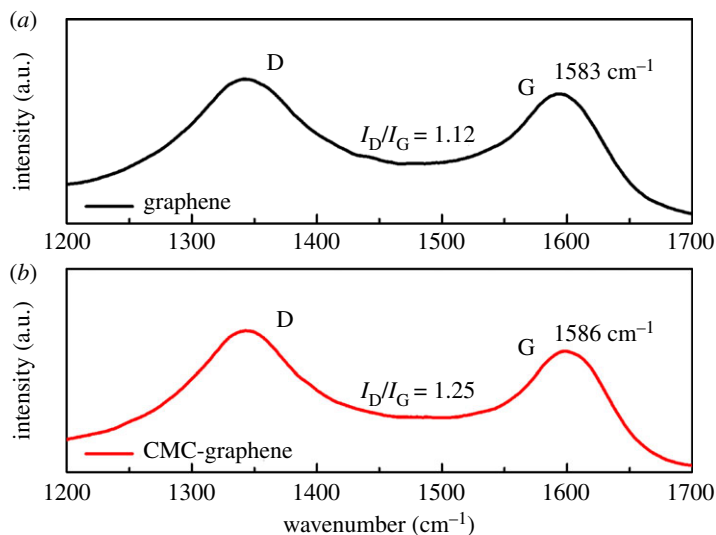
Figure 1. Raman spectra of (*a*) pristine graphene sheets and (*b*) CMC–graphene sheets.
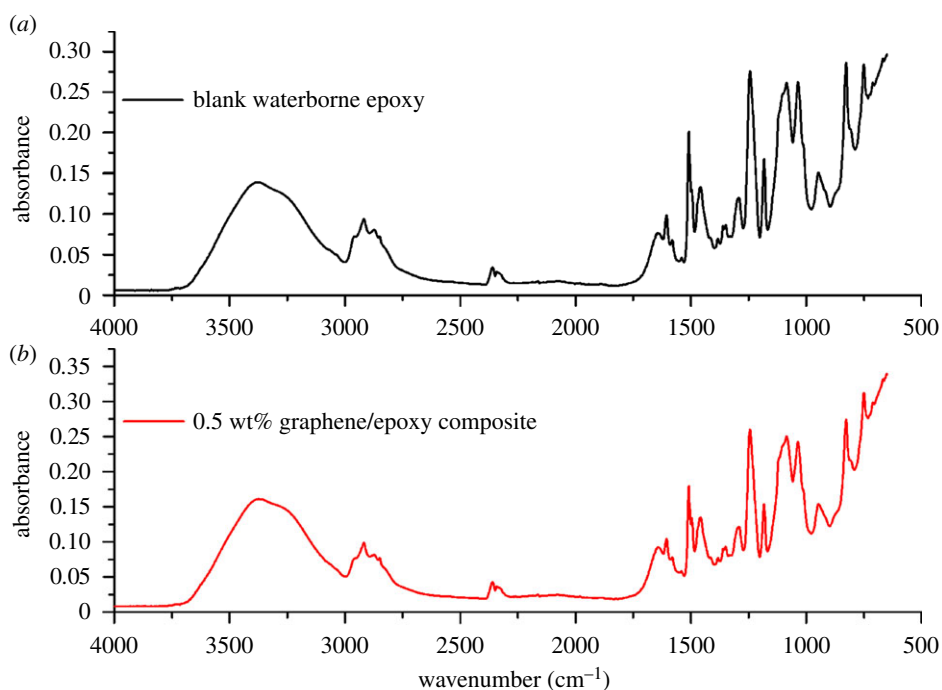

Figure 2. FTIR spectra of (*a*) blank waterborne epoxy coating and (*b*) 0.5 wt% graphene/waterborne epoxy composite coating.

CMC–graphene. This suggested that the degree of disorder for the CMC–graphene sheets was higher than that for the pristine graphene.

FTIR spectroscopy was also used to analyse the interaction between the graphene sheets and epoxy matrix. Figure 2*a* shows the FTIR spectrum of the blank waterborne epoxy coating. Absorption peaks at 1606 cm^{-1} and 1508 cm^{-1} are owing to stretching vibrations of the phenyl ring. The peak near 2800–3000 cm^{-1} is owing to the C–H vibration of the aliphatic group. The peak in 1244 cm^{-1} and the broad absorption at 3382 cm^{-1} are assigned to C–O–C and –OH respectively. Absorption at 916 cm^{-1} and 827 cm^{-1} are assigned to epoxy groups. Figure 2*b* shows the FTIR spectrum of the 0.5 wt% graphene/waterborne epoxy composite coating. Introducing graphene did not evidently result in new functional groups. This indicated that graphene was physically dispersed in the epoxy matrix without chemical modification.

The microscopic morphology of pristine graphene was investigated by SEM, as shown in figure 3*a*. The flake structure of pristine graphene was clearly observed. Agglomeration and stacking were also observed, which may result in degradation of the properties of graphene. The dispersion of graphene was investigated by TEM. Figure 3*b* and *c* shows TEM images of the dispersion of untreated pristine
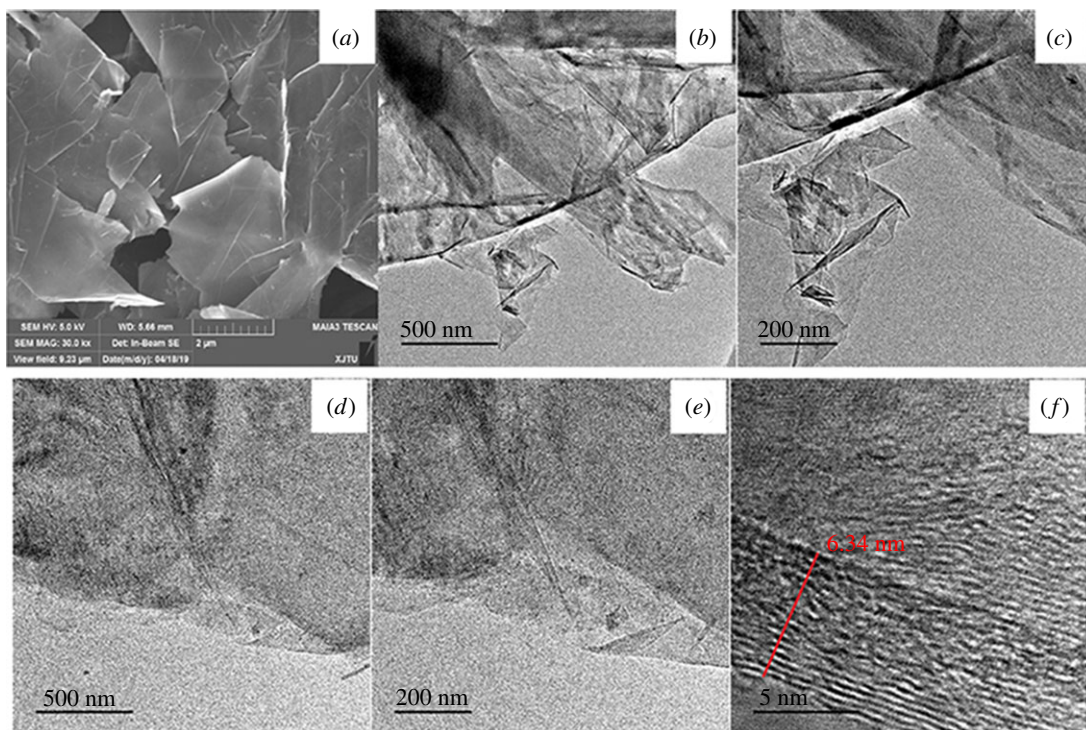
Figure 3. (*a*) SEM image of pristine graphene; (*b,c*) TEM images of pristine graphene; (*d,e,f*) TEM images of graphene dispersed by CMC.
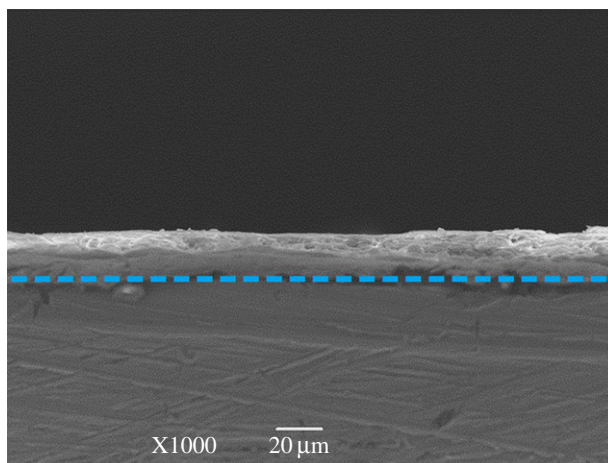

Figure 4. The cross-sectional SEM image of 0.5 wt% graphene/waterborne epoxy composite coating on the steel 1020 test surface.

graphene. The untreated graphene sheets were highly agglomerated and showed many wrinkles. TEM images of graphene dispersed by CMC are shown in figure 3*d*–*f*. A thin film was observed with no obvious aggregation and far less wrinkled surfaces. The high-resolution TEM image in figure 3*f* shows the average thickness of the CMC–graphene is about 6–7 nm. This indicated that monolayer or few-layer graphene sheets were obtained by CMC dispersion.

Based on the above characterization, waterborne epoxy coatings with graphene dispersed by CMC were expected to exhibit better corrosion resistance performance than those with pristine graphene. Therefore, composite coatings mentioned in the following discussion refer to waterborne epoxy coatings containing CMC–graphene. The graphene/waterborne epoxy composite was coated on the test surface of the steel 1020 using a wire bar coater. The thickness of the coating was investigated by SEM. The SEM image in figure 4 suggested that a uniform graphene/waterborne epoxy composite coating with a thickness of 20 ± 2 µm was successfully obtained on the test surface of the working electrode.

Figure 5 shows SEM images of the surface topography of the blank epoxy coating and 0.5 wt% graphene/waterborne epoxy composite coating. The SEM image of the blank waterborne epoxy coating in figure 5*a* shows a surface topography containing many pores and inhomogeneous defects that is owing to the rapid water evaporation during the curing process of waterborne epoxy coatings.
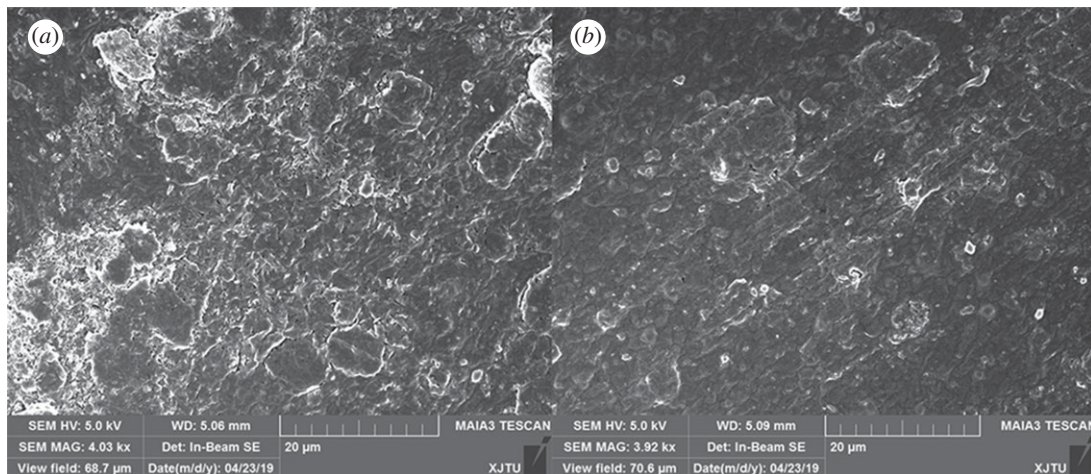
Figure 5. SEM images of the surface topography of (*a*) blank epoxy coating and (*b*) 0.5 wt% graphene/waterborne epoxy composite coating.
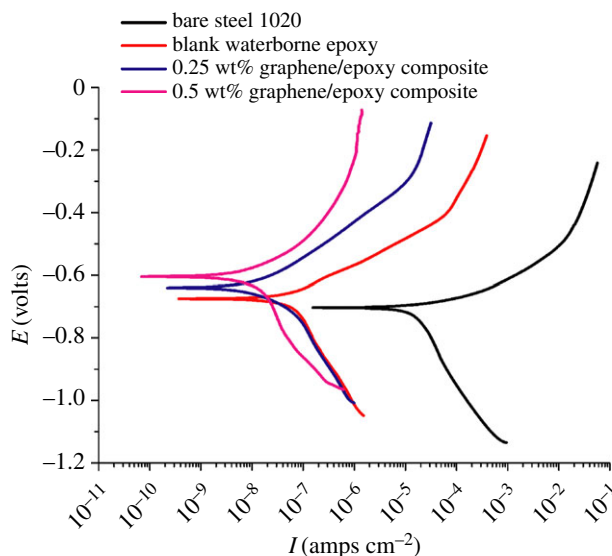

Figure 6. Polarization curves of the bare, blank waterborne epoxy, 0.25 wt% graphene/epoxy composite and 0.5 wt% graphene/epoxy composite-coated electrodes in CO_2-satarated 10 wt% NaCl solution after 2 h of immersion.

These pores and defects will serve as active channels for aggressive species, and it is not surprising that the corrosion resistance of waterborne epoxy coatings are significantly lower than those of solvent-based epoxy coatings. The SEM image of the waterborne epoxy coating incorporating graphene in figure 5*b* showed a more uniform and smooth surface with far fewer cracks. This is because the graphene was well dispersed in the epoxy matrix, which blocked the diffusion pathways and slowed the evaporation of water [26]. The graphene/waterborne epoxy composite coating could therefore retard the permeation of corrosive medium and potentially improve the corrosion resistance performance.

3.2. Polarization curve measurements

The polarization curves of bare steel 1020 and steel 1020 coated with blank waterborne epoxy, 0.25 wt% and 0.5 wt% graphene/waterborne epoxy composite after immersion in CO_2-satarated 10 wt% NaCl solution for 2 h at 25°C are shown in figure 6. The parameters obtained from the Tafel extrapolation method are shown in table 2, in which I_{corr} and E_{corr} stand for the corrosion current density and the corrosion potential respectively. B_a and B_c represent the slope of the anodic and cathodic polarization, respectively. η stands for the inhibition efficiency calculated by equation (3.1):

$$\eta = 1 - \frac{I'_{corr}}{I^0_{corr}}, \tag{3.1}$$

Table 2. Parameters obtained from polarization curves in figure 6.

	bare steel 1020	blank waterborne epoxy	0.25%wt graphene/epoxy composite	0.5%wt graphene/epoxy composite
corrosion rate (mm a^{-1})	0.381	7.93×10^{-4}	1.64×10^{-4}	4.99×10^{-5}
I_{corr} (amps cm^{-2})	3.73×10^{-5}	6.74×10^{-8}	1.39×10^{-8}	4.24×10^{-9}
E_{corr} (volts)	-0.705	-0.676	-0.639	-0.604
B_a (mV dec^{-1})	41.3	84.7	128	167
B_c (mV dec^{-1})	-357	-329	-289	-345
η	—	99.79%	99.96%	99.98%

where I_{corr}^0 stands for the corrosion current density of the uncoated steel 1020. I'_{corr} represents the corrosion current density of the coated electrode [27]. The E_{corr} of the 0.5 wt% graphene/epoxy composite coating (-0.604 V) was more positive than that of the blank waterborne epoxy coating (-0.676 V), which showed that adding graphene lowered the corrosion tendency. The anodic and cathodic polarization current densities of the 0.25 wt% graphene/epoxy composite coating were around 2–3 orders of magnitude lower than that of bare 1020 steel with $\eta = 99.96\%$. When graphene was added with a mass fraction of 0.5%, the corrosion rate was further reduced compared with that of the 0.25 wt% graphene/epoxy composite coating with $\eta = 99.98\%$. Table 1 shows that B_a increased with the addition of graphene while B_c did not change significantly. The increase of B_a indicates the transition of anodic reaction. With the addition of graphene, the intensity of the Fe element of graphene/epoxy composite coating at the interface of the substrate metal and the composite coating is stronger than that of the pure epoxy coating, and the increase in the intensity of Fe element indicates the deposition of iron ions at the interface [28]. Therefore, the graphene distributed inside the composite coating was thought to impede the diffusion of Fe ions which retarded the anodic reaction.

3.3. Electrochemical impedance spectroscopy measurements

EIS measurements were used to study the resistance and porosity of the coatings. Figure 7 shows Bode plots of the blank waterborne epoxy, 0.25 wt% and 0.5 wt% graphene/waterborne epoxy composite coatings after an initial period of immersion of 0−90 min. All coatings exhibit only one time constant in the high-frequency range, which corresponds to the capacitance of the coating within 30 min of immersion time. In this period, the coating is equivalent to an insulating layer with a large resistance and small capacitance, which isolates moisture from the base metal [29].

With the increase of immersion time, the second time constant associated with the capacitance of a double layer appears in the low-frequency range, as shown in figure 7a. It shows that the corrosion medium has penetrated into the interface and forms a double layer between the blank waterborne epoxy coating and the substrate metal after 90 min of immersion time.

In comparison, the appearance of the second time constant in the low-frequency range for the 0.25 wt% graphene/waterborne epoxy composite coating was delayed, while the second time constant for the 0.5 wt% graphene composite coating hardly appeared. This indicates that the permeation of the corrosive medium was inhibited.

Figure 8 shows Nyquist plots of the blank waterborne epoxy coating and composite coatings during 96 h of immersion time. The EIS profiles for the composite coatings at various immersion times showed two capacitive loops. For the blank waterborne epoxy coating in figure 8a, the radii of the two capacitive loops decreased dramatically with increasing immersion time and then stabilized after 72 h. This indicated poor water isolating properties of the blank epoxy coating.

For the 0.25 wt% graphene/waterborne epoxy composite coating in figure 8b, the radii of the two capacitive loops were larger than those of the blank waterborne epoxy coating. However, the impedance modulus still decreased significantly during the 96 h of immersion.

The impedance modulus of the 0.5%wt graphene/waterborne epoxy composite coating in figure 8c was around two orders of magnitude higher than that of the blank waterborne epoxy coating. The radii of the two capacitive loops remained relatively constant during the overall immersion time. This
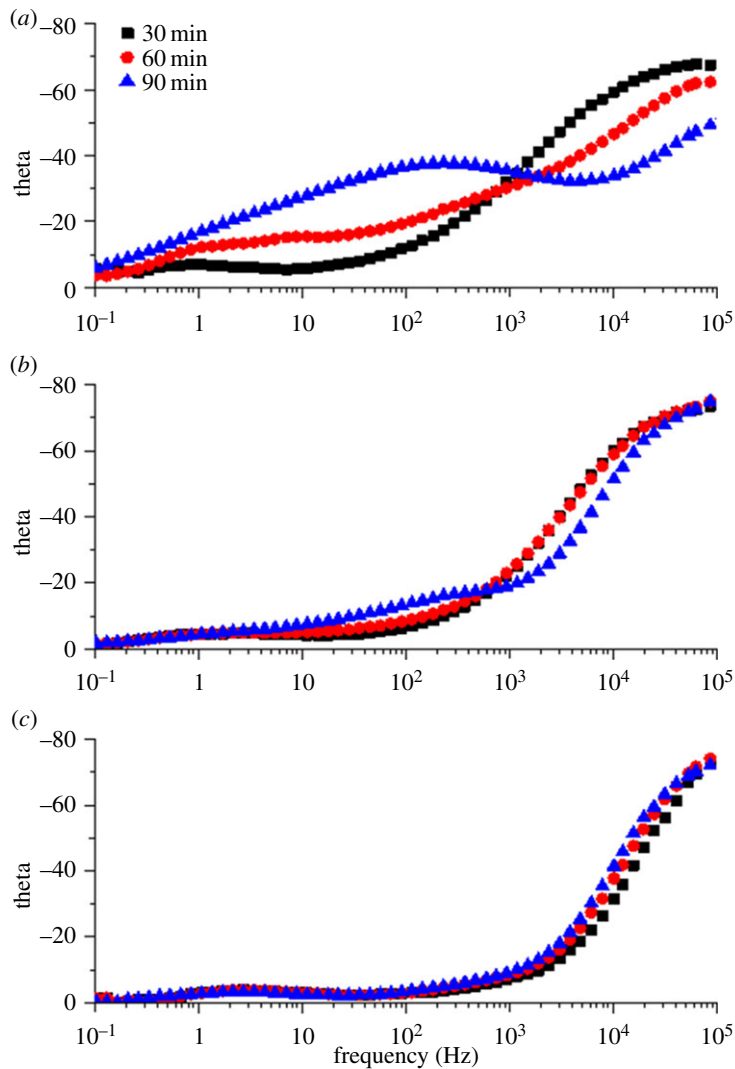
Figure 7. Bode plots (phase angle, theta) of (*a*) blank waterborne epoxy coating, (*b*) 0.25 wt% graphene/waterborne epoxy composite coating and (*c*) 0.5 wt% graphene/waterborne epoxy composite coating in CO_2-satarated 10 wt% NaCl solution for immersion times of 30–90 min.

indicated the anti-corrosion properties of the composite coating were improved with the addition of graphene content. The composite coating provided effective corrosion protection for the substrate metal during long-term immersion.

Figure 9 shows the equivalent circuit diagram of the EIS profiles, where R_s and R_c stand for the solution resistance and the coating resistance, respectively. R_{ct} is the charge transfer resistance. Q_c is the capacitance of the coating. Q_{dl} is the capacitance of the double layer. The fitting data are shown in table 3. The R_c values for all coating systems decreased and the Q_c values for all coating systems gradually increased with increasing immersion time. This was mainly owing to the gradual penetration of water molecules and corrosive Cl^- with strong polarity and high dielectric constant into the coating. The R_{ct} values decreased with increasing immersion time, because water molecules, CO_2 and Cl^- penetrated through the interface between the coating and the base steel, accelerating the corrosion of the steel during immersion.

After 96 h of immersion, the Q_c of the pure epoxy, 0.25 wt% and 0.5 wt% graphene/waterborne epoxy composite coatings were 6.11 µF cm^{-2}, 6.34×10^{-4} µF cm^{-2} and 1.17×10^{-3} µF cm^{-2}, respectively. This indicated that graphene enhanced the coatings compactness and prevented the diffusion of corrosive media into the coating. The R_c of the blank epoxy composite decreased from 9.70 kΩ cm^2 to 0.455 kΩ cm^2, the R_c of the 0.25 wt% graphene/waterborne epoxy composite decreased from 45.2 kΩ cm^2 to 20.9 kΩ cm^2, while the R_c of the 0.5 wt% composite coating decreased from 227 kΩ cm^2 to 117 kΩ cm^2 within 96 h of immersion. This indicated that corrosion resistance of the composite
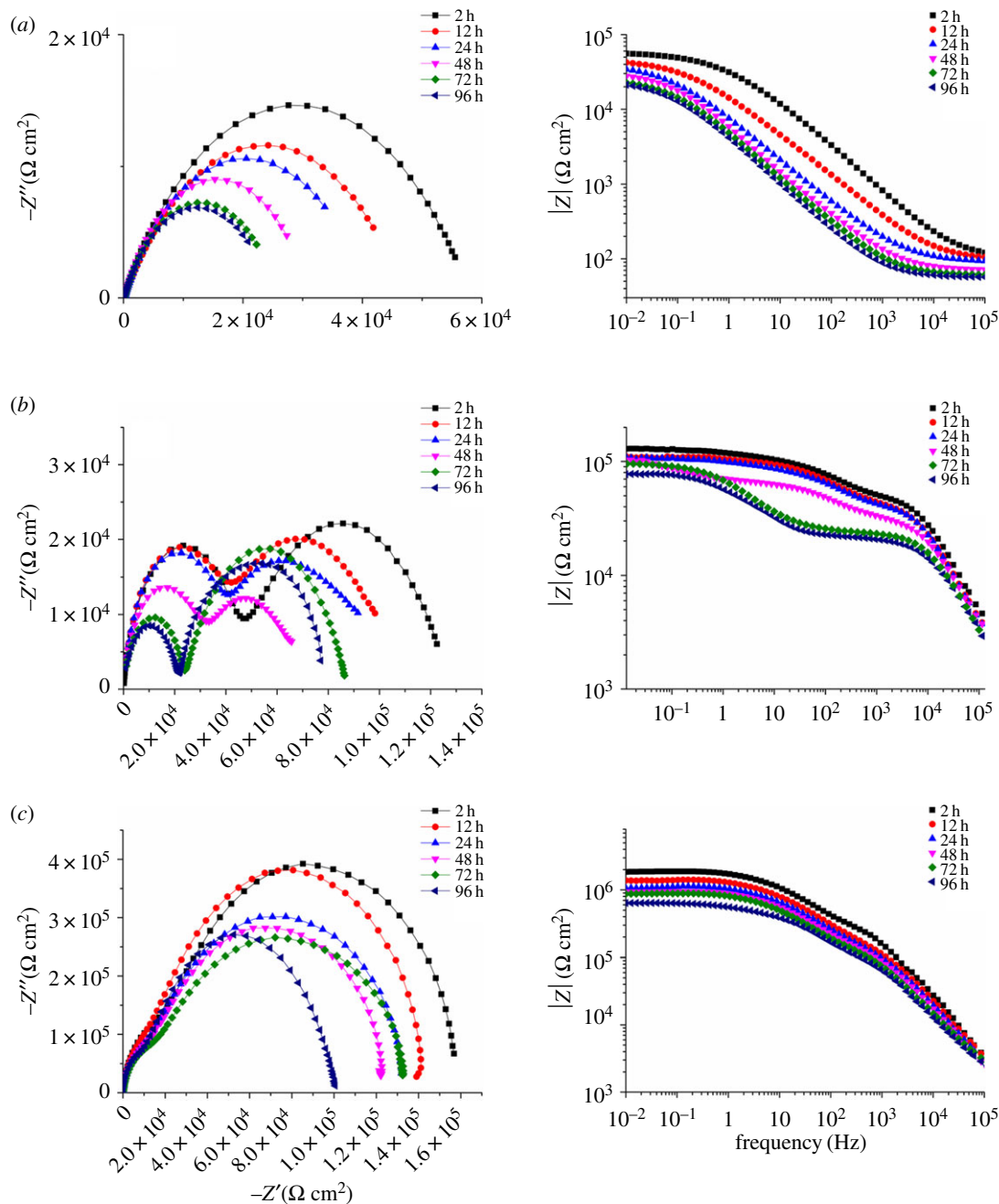
Figure 8. Nyquist plots of the (*a*) blank waterborne epoxy coating, (*b*) 0.25 wt% graphene/waterborne epoxy composite coating and (*c*) 0.5 wt% graphene/waterborne epoxy composite coating in CO_2-saturated 10 wt% NaCl solution for immersion times of 2–96 h.
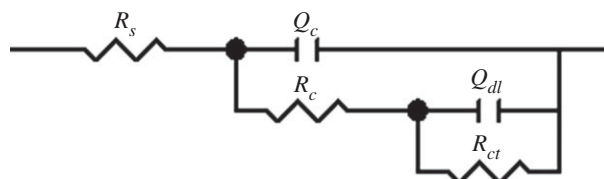

Figure 9. Equivalent circuit diagram of the EIS profiles.

coatings gradually increased and remained relatively constant with addition of graphene content. The R_{ct} of the 0.5 wt% graphene/waterborne epoxy composite coating (896 kΩ cm^2) was much higher than that of the pure epoxy coating (24.6 kΩ cm^2). R_{ct} reflects the difficulty of electron transfer across the interface between electrodes and electrolyte solutions. The addition of graphene increased the resistance of the corrosion reaction of the metal.
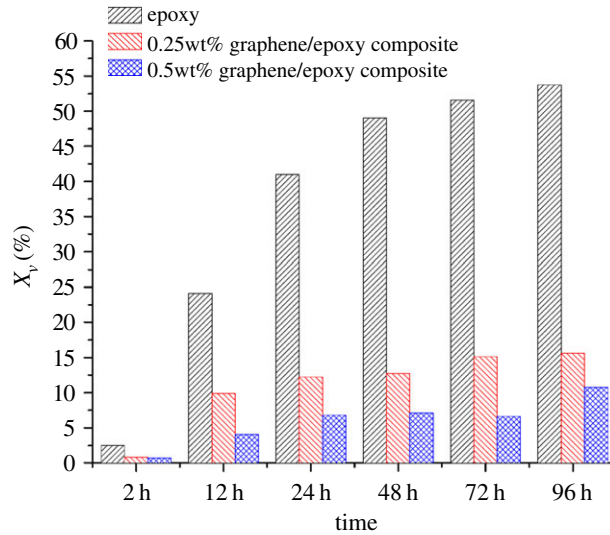
Figure 10. Water absorption volume percentage of the different coatings after increasing immersion times.

Table 3. Fitting results from the EIS measurements in figure 8.

	time/h	$R_s/$ $(\Omega\ cm^2)$	$Q_c/$ $(\mu F\ cm^{-2})$	$R_c/$ $(k\Omega\ cm^2)$	$Q_{dl}/(\mu F\ cm^{-2})$	$R_{ct}/$ $(k\Omega\cdot cm^2)$
epoxy	2	4.23	0.647	9.70	1.03	48.5
	12	4.29	1.67	3.82	6.27	43.3
	24	3.79	3.49	1.33	14.5	39.8
	48	4.86	4.97	0.961	19.3	30.3
	72	4.46	5.56	0.687	28.3	25.2
	96	3.99	6.11	0.445	40.2	24.6
0.25% wt graphene/epoxy composite	2	3.32	3.30×10^{-4}	45.2	2.71×10^{-2}	82.04
	12	4.28	4.94×10^{-4}	42.7	5.63×10^{-2}	69.91
	24	4.37	5.47×10^{-4}	39.3	3.94×10^{-2}	60.52
	48	4.96	5.59×10^{-4}	30.0	6.17×10^{-2}	42.43
	72	3.92	6.21×10^{-4}	23.5	1.64	93.87
	96	4.75	6.34×10^{-4}	20.9	1.85	60.01
0.5% wt graphene/epoxy composite	2	3.98	7.53×10^{-4}	227	1.26×10^{-2}	1371
	12	3.78	8.72×10^{-4}	161	1.38×10^{-2}	1290
	24	4.45	9.83×10^{-4}	156	1.60×10^{-2}	1192
	48	4.60	9.97×10^{-4}	142	1.71×10^{-2}	1091
	72	4.65	9.76×10^{-4}	122	1.83×10^{-2}	1166
	96	4.87	1.17×10^{-3}	117	2.55×10^{-2}	896

According to the theory of Brasher and Kingsbury, equation (3.2) can be applied to calculate the water absorption volume percentages of the different coatings [30]:

$$X_v\% = 100 \cdot \frac{\log(C_c(t)/C_c(0))}{\log(80)}, \tag{3.2}$$

where X_v is the water absorption volume percentage of the organic coating, and $C_c(0)$ and $C_c(t)$ are the coating capacitances after immersion for time 0 and time t, respectively. In this study, the value of $C_c(0)$ was obtained by the fitting results of EIS measurements for an immersion time of 30 min. The stability of

the water absorption volume percentage can be used to judge whether the performance of the coating is stable. The calculation results are shown in figure 10. The X_v ($t = 96$ h) for the blank epoxy coating, 0.25 wt% and 0.5 wt% graphene/waterborne epoxy composite coating were 53.7%, 15.6% and 10.8%, respectively. The water absorption of epoxy coating decreased significantly with increasing graphene content, and the performance of all the coating systems stabilized after 96 h of immersion. We therefore concluded that the composite coating prevented the diffusion of water into the coating and provided durable and effective anti-corrosion protection for the substrate metal.

4. Conclusion

Graphene/waterborne epoxy composite coatings with different mass fractions of graphene were prepared to investigate their corrosion resistance in CO_2-satarated NaCl solution. Composite coatings with more uniform surfaces and far fewer defects than blank waterborne epoxy coatings were obtained on 1020 steel. The electrochemical characterizations proved improved corrosion resistance of waterborne epoxy coatings by adding graphene. The 0.25 wt% graphene/epoxy composite coating provided an inhibition efficiency $\eta = 99.96\%$, while further improvement was achieved by increasing the content of graphene additive to 0.5 wt%. The anodic dissolution reaction was retarded by the graphene distributed inside the composite coating, which acted as an effective barrier and suppressed the diffusion of Fe ions. The increase in coating resistance and decrease in water absorption volume percentage of the graphene/waterborne epoxy composite coatings showed that they provided durable and effective protection for the substrate metal in CO_2-satarated NaCl solution.

References

1. Gozalpour F, Ren SR, Tohidi B. 2005 CO_2 eor and storage in oil reservoir. *Oil Gas Sci. Technol.* **60**, 537–546. (doi:10.2516/ogst:2005036)

2. Li T, Wu H, Li X. 2008 CO_2 corrosion of natural gas pipe steels. *Corros. Prot.* **29**, 260.

3. Bockris JO'M, Khan SU. 1993 *Surface electrochemistry: a molecular level approach*, p. 756. New York, NY: Plenum Press.

4. Popoola LT, Grema AS, Latinwo GK, Gutti B, Balogun AS. 2013 Corrosion problems during oil and gas production and its mitigation. *Int. J. Ind. Chem.* **4**, 35. (doi:10.1186/2228-5547-4-35)

5. Prabha SS, Rathish RJ, Dorothy R, Brindha G, Pandiarajan M, Al-Hashem A, Rajendran S. 2014 Corrosion problems in petroleum industry and their solution. *Eur. Chem. Bull.* **3**, 300–307. (doi:10.17628/ECB.2014.3.300)

6. Lutzler T et al. 2018 Evaluation and characterization of anti-corrosion properties of sol-gel coating in CO_2 environments. *Mater. Chem. Phys.* **216**, 272–277. (doi:10.1016/j.matchemphys.2018.06.005)

7. Li W, Pots BFM, Kang X, Nesic S. 2017 Inhibition of CO_2 corrosion of mild steel — study of mechanical effects of highly turbulent disturbed flow. *Corros. Sci.* **126**, 208–226. (doi:10.1016/j.corsci.2017.07.003)

8. Xiang Y, Long Z, Li C, Huang H, He X. 2017 Inhibition of N80 steel corrosion in impure supercritical CO_2 and CO_2-saturated aqueous phases by using imino inhibitors. *Int. J. Greenh. Gas Con.* **63**, 141–149. (doi:10.1016/j.ijggc.2017.05.010)

9. Guo S, Xu L, Zhang L, Chang W, Lu X. 2012 Corrosion of alloy steels containing 2% chromium in CO_2 environments. *Corros. Sci.* **63**, 246–258. (doi:10.1016/j.corsci.2012.06.006)

10. Guo S, Xu L, Zhang L, Chang W, Lu X. 2016 Characterization of corrosion scale formed on 3Cr steel in CO_2-saturated formation water. *Corros. Sci.* **110**, 123–133. (doi:10.1016/j.corsci.2016.04.033)

11. Bohm S. 2014 Graphene against corrosion. *Nat. Nano Technol.* **9**, 741–742. (doi:10.1038/nnano.2014.220)

12. Chen S et al. 2011 Oxidation resistance of graphene-coated Cu and Cu/Ni alloy. *ACS Nano* **5**, 1321–1327. (doi:10.1021/nn103028d)

13. Prasai D, Tuberquia JC, Harl RR, Jennings GK, Bolotin KI. 2012 Graphene: corrosion-inhibiting coating. *ACS Nano* **6**, 1102–1108. (doi:10.1021/nn203507y)

14. Kirkland NT, Schiller T, Medhekar N, Birbilis N. 2012 Exploring graphene as a corrosion protection barrier. *Corros. Sci.* **56**, 1–4. (doi:10.1016/j.corsci.2011.12.003)

15. Wang Y, Zheng Y, Xu X, Dubuisson E, Bao Q, Lu J, Loh KP. 2011 Electrochemical delamination of CVD-grown graphene film: toward the recyclable use of copper catalyst. *ACS Nano* **5**, 9927–9933. (doi:10.1021/nn203700w)

16. Raman RS et al. 2012 Protecting copper from electrochemical degradation by graphene coating. *Carbon* **50**, 4040–4045. (doi:10.1016/j.carbon.2012.04.048)

17. Schriver M, Regan W, Gannett WJ, Zaniewski AM, Crommie MF, Zettl A. 2013 Graphene as a long-term metal oxidation barrier: worse than nothing. *ACS Nano* **7**, 5763–5768. (doi:10.1021/nn4014356)

18. Chang CH, Huang TC, Peng CW, Yeh TC, Lu HI, Hung AWI, Weng CJ, Yang TI, Yeh JM. 2012 Novel anticorrosion coatings prepared from polyaniline/graphene composites. *Carbon* **50**, 5044–5051. (doi:10.1016/j.carbon.2012.06.043)

19. Ye Y, Zhang D, Liu T, Liu Z, Liu W, Pu J, Li X. 2019 Improvement of anticorrosion ability of epoxy matrix in simulate marine environment by filled with superhydrophobic POSS-GO nanosheets. *J. Hazard. Mater.* **364**, 244–255. (doi:10.1016/j.jhazmat.2018.10.040)

20. Liu S, Gu L, Zhao H, Chen J, Yu H. 2016 Corrosion resistance of graphene-reinforced waterborne epoxy coatings. *J. Mater. Sci. Technol.* **32**, 425–431. (doi:10.1016/j.jmst.2015.12.017)

21. Ye Y, Zhang D, Liu T, Liu Z, Pu J, Liu W, Zhao H, Li X, Wang L. 2019 Superior corrosion resistance and self-healable epoxy coating pigmented with silanzied trianiline-intercalated graphene. *Carbon* **142**, 164–176. (doi:10.1016/j.carbon.2018.10.050)

22. Yang T, Cui Y, Li Z, Zeng H, Luo S, Li W. 2018 Enhancement of the corrosion resistance of epoxy coating by highly stable 3, 4, 9, 10-perylene tetracarboxylic acid functionalized graphene. *J. Hazard. Mater.* **357**, 475–482. (doi:10.1016/j.jhazmat.2018.06.038)

23. Liao R, Tang Z, Lei Y. 2011 Polyphenol-reduced graphene oxide: mechanism and derivatization. *J. Phys. Chem. C* **115**, 20 740–20 746. (doi:10.1021/jp2068683)

24. Liang Y, Wu D, Feng X. 2009 Dispersion of graphene sheets in organic solvent supported by ionic interactions. *Adv. Mater.* **21**, 1679–1683. (doi:10.1002/adma.200803160)

25. Kamada S, Nomoto H, Fukuda K, Fukawa T, Shirai H, Kimura M. 2011 Noncovalent wrapping of chemically modified graphene with π-conjugated disk-like molecules. *Colloid. Polym. Sci.* **289**, 925–932. (doi:10.1007/s00396-011-2414-z)

26. Zhou S, Wu Y, Zhao W, Yu J, Jiang F, Ma L. 2018 Comparative corrosion resistance of graphene sheets with different structures in waterborne epoxy coatings. *Colloid. Surface. A* **556**, 273–283. (doi:10.1016/j.colsurfa.2018.08.045)

27. Wu S, Chen Z, Qiu Y, Guo X. 2012 Corrosion protection of copper by self-assembled monolayers modified in aqueous micellar solution. *J. Electrochem. Soc.* **159**, C277–C282. (doi:10.1149/2.013207jes)

28. Hu HJ, Xu H, Li YJ, Chen X, Li Y. 2019 Study of CO_2 corrosion behavior of graphene/epoxy composite coating in high chloride environment. Corrosion NACE. Paper No.13212. Houston, TX: NACE International.

29. Cao CN, Zhang JQ. 2002 *An introduction to electrochemical impedance spectroscopy*, p. 156. Beijing, China: Science Press.

30. Brasher DM, Kingsbury AH. 1954 Electrical measurements in the study of immersed paint coatings on metal. I. Comparison between capacitance and gravimetric methods of estimating water-uptake. *J. Appl. Chem.* **4**, 62–72. (doi:10.1002/jctb.5010040202)

31. Xu H, Hu H, Wang H, Li Y, Li Y. 2020 Data from: Corrosion resistance of graphene/ waterborne epoxy composite coatings in CO_2-satarated NaCl solution. Dryad Digital Repository. (https://doi.org/10.5061/dryad.mkkwh70vk)